Article

Design and Simulation of a New Near Zero-Wear Non-Contact Self-Impact Seal Based on the Tesla Valve Structure

Yan Wang [1,2,3,*], Yiming He [1], Xuefei Xie [1], Zhouxin Huang [1], Hui Xu [1], Qiong Hu [1] and Chenbo Ma [4]

[1] School of Mechanical Engineering, Jiangsu Ocean University, Lianyungang 222005, China
[2] Jiangsu Institute of Marine Resources Development, Lianyungang 222005, China
[3] School of Mechatronic Engineering, China University of Mining and Technology, Xuzhou 221116, China
[4] College of Mechanical Engineering, Nanjing Forestry University, Nanjing 210037, China
[*] Correspondence: wy_seal@jou.edu.cn

Abstract: This study proposes a new near zero-wear non-contact self-impact seal based on the passive fluid blocking principle and the Tesla valve structure, which is characterised by near zero-wear, a long lifetime, a simple structure and high stability. Research shows that the impact-blocking effect of a three-dimensional leakage channel can realise the stepwise throttling effect of the sealing medium. Furthermore, the pressure, number of seal stages and seal spacing significantly affect leakage. Leakage can be effectively controlled by increasing seal series and reducing seal spacing. The proposed near zero-wear impact seal is more suitable for the gas medium. Compared with the conventional sealing form, the new seal is simplified significantly. Large spacing and fixed design can significantly improve the ability to seal pairs to resist vibration and impact during operation, and the sealing performance is not restricted by the rotation speed. The form of the proposed seal will enable a new non-contact mechanical seal technology and a new structure to be developed, thereby advancing the existing seal field.

Keywords: non-contact mechanical seal; near zero-wear; Tesla valve; seal structure; numerical analysis

1. Introduction

The non-contact mechanical seal based on hydrodynamic lubrication exhibits the characteristics of near zero-wear, low power consumption and long life. It has been developed rapidly and prioritised advanced sealing technology research and development [1,2]. Currently, non-contact mechanical seals primarily include a labyrinth [3], dry gas [4], upstream pumping [5], spiral [6], clearance [7], centrifugal [8] and magnetic fluid seals [9], while the lubrication mode between the sealing rings is a gas or liquid film. However, most non-contact mechanical seals are not perfect. In particular, the encountered issues are as follows: ① a straight-through breathable effect occurs in the sealing structure, resulting in considerable leakage and low sealing efficiency (e.g., labyrinth, dry gas, spiral and clearance seals); ② over-dependence on the rotation speed—during the start and stop stages, the seal will lose its sealing ability (e.g., dry gas, centrifugal and upstream pumping seals); ③ weak adaptability to high-speed or high-pressure conditions (e.g., magnetic fluid and spiral seals); and ④ complex auxiliary devices, low system stability (e.g., dry gas, upstream pumping and screw seals). Despite the disadvantages mentioned above, considering that the viscosity of gas is approximately one-thousandth that of liquid, a non-contact seal without solid friction still offers a more efficient form of sealing for high parameter conditions. If we can further improve throttling efficiency by innovating fluid blocking mechanism on the basis of non-contact operation, avoid the over-dependence of sealing performance on speed or restricted by speed, while considering the characteristics of simple structure and high stability, it can be regarded as a technical innovation in the field of non-contact sealing.

Inspired by the passive fluid control principle and single guide pass characteristics of the Tesla valve, the structure was extended from a two-dimensional plane form to a three-dimensional cylinder in this study; additionally, the single guide pass characteristic had been upgraded for the unidirectional (from high to low-pressure sides) leakage suppression of the seal. This study aims to reveal the leakage suppression mechanism of the fluid impact blocking effect via the macroscopic reconstruction of the mesoscopic leakage channel in a model. Unlike the conventional non-contact seal, the proposed seal exhibits the characteristics of high efficiency, near zero-wear and high stability simultaneously, which allow efficient non-contact sealing technology to be realised.

2. Tesla Valve and Its Structural Improvements

2.1. Tesla Valve Structure and Operating Principle

The tesla valve is a single guide pass valve proposed by Nikola Tesla [10] (see Figure 1). The structure does not involve any moving components, requires no energy input and only uses a spatial structure to push or suppress fluid flow [11,12]. The difference between forward flow (from right to left) and reverse flow (from left to right) is significant. In the forward flow, the fluid can flow unimpeded from right to left, bypassing all winglike barriers; furthermore, the fluid acceleration effect can be achieved because of the flow pressure effect. However, in the reverse flow, the fluid enters a winglike barrier up/down each passage, creating a severe impact blockage at the intersection of the bend and the horizontal pipe. The more the number of winglike barriers, the greater the resistance of the fluid from propelling forward, which results in the unique self-impact single guide characteristics of the Tesla valve structure. Tesla himself presented the following concept: assuming that the leakage rate of fluid through the first winglike barrier is expressed as a fraction $1/X$, after the n-th winglike barrier, the leakage is only $(1/X)n$. X need not be a high number to ensure a near-perfect valve throttling behaviour.
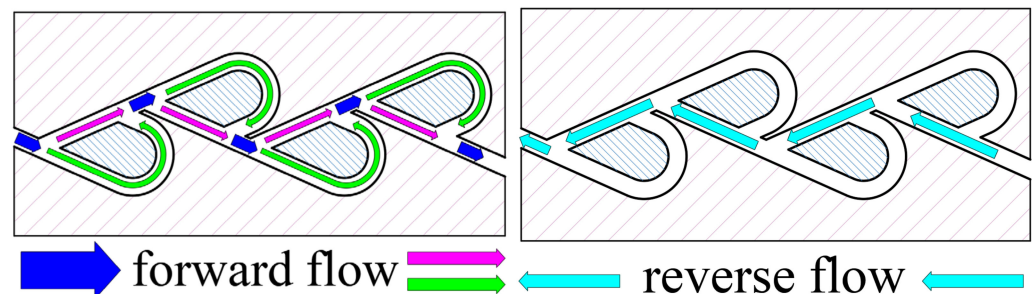

**Figure 1.** Schematic diagram of the Tesla valve.

Although the Tesla valve has been proposed, its application is rarely investigated. In fact, the unique structure of the Tesla valve has only been highlighted and applied in recent years. In 2003, Truong et al. [13] proposed a comprehensive optimisation method for the complete design and system optimisation of the structural parameters of the Tesla valve. In 2005, Gamboa et al. [14] geometrically optimised the Tesla valve based on six independent design variables, thereby increasing the resistance ratio by 25%. In 2011, Thompson et al. [15] applied the Tesla valve to the verify the valve design of a flat plate oscillating heat pipe, which indicated reduced resistance by 15–25% compared to the conventional check valve. Subsequently, Thompson et al. [16] investigated a multistage Tesla check valve and the results showed that the multistage structure afforded a higher single guide pass efficiency, which increased significantly with the Reynolds number. In 2014, Wang et al. [17] applied this structure to a Micromixer, which effectively reduced the pressure drop and significantly improved the mixing efficiency. In 2017, Vries et al. [18] successfully designed a new pulsating heat pipe valve based on the Tesla valve structure; it facilitated fluid circulation and significantly reduced thermal resistance efficiency. In 2018, Qian et al. [19–21] confirmed that the Tesla valve is applicable on the ion flow scale and successfully applied it to the decompression process of hydrogen fuel cells. The proposed

multistage Tesla valve afforded good decompression effects. In 2020, Wahidi et al. [22] applied the Tesla valve in a supercritical CO_2 cycle circuit, thereby alleviating temperature and velocity oscillations and allowing the system to achieve higher supercritical pressures and heat inputs. In 2021, Monika et al. [23] proposed a liquid cooling plate comprising a Tesla valve, which can provide a safe temperature range for bag-type lithium batteries. In 2022, Shi et al. [24] introduced the Tesla valve structure into the design of sweat collection chips, which improved collection efficiency and prevented inlet backflow.

The studies above show that the unique structure of the Tesla valve has gained increasing attention as well as keen interest from scholars in various fields. Unlike the abovementioned applications, the sealing function design based on the single guide pass characteristics of the Tesla valve structure was attempted in this study. Theoretically, if a sufficient number of throttling channels are available, then a stable blocking seal with no moving components and a near zero-wear non-contact form can be achieved by progressively establishing blocking areas.

2.2. Proposed Near Zero-Wear Non-Contact Self-Impact Seal

In this study, a new sealing structure design (named self-impact seal) was established based on the single guide pass characteristics of the Tesla valve, the main channel of which adopts a step design while considering the assembly relationship of each component, as shown in Figure 2. The structure of the seal is simple in terms of composition, i.e., it includes only three components— an outer ring, a suspending pillar and an inner ring. The inner ring rotates simultaneously with the shaft. In addition, no other additional moving components are included. Furthermore, the outer ring can directly rely on the sealing end cover or machine housing and the suspending pillar can be fixed in the inner ring or outer ring via the built-in screws and double-headed studs. Similar to the two-dimensional Tesla valve, a space composed of a suspending pillar and the corresponding inner and outer rings is used in the seal stage. The outlet and inlet ends are located on the atmospheric and high-pressure sides of the sealing medium, respectively.
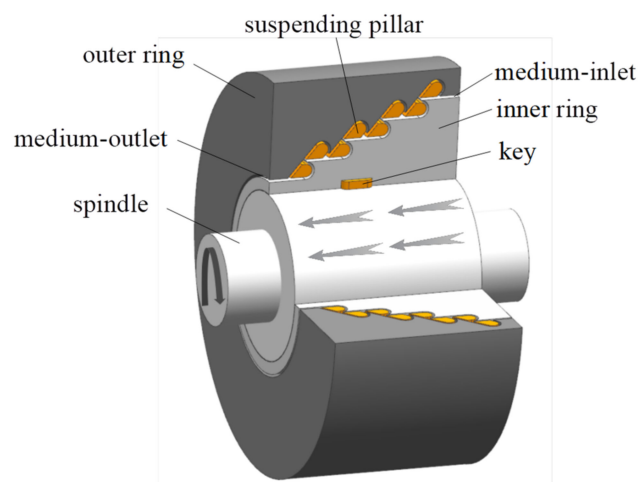

Figure 2. Three-dimensional structure drawing of the self-impact seal.

### 2.3. Structure Optimization

2.3.1. Geometric Model

The single-stage size structure is shown in Figure 3a, where R is the turning radius, l the flow distance and α the diversion angle; furthermore, R, l and α are mutually restricted. In the model, each seal stage is of the same size, with the high- and low-pressure inlets located on the left and right, respectively. Multiple seal stages are connected to form a sealed three-dimensional leakage channel (designed by UG software), as shown in Figure 3b. Theoretically, a larger pressure difference necessitates more seal stages and a larger axial size.
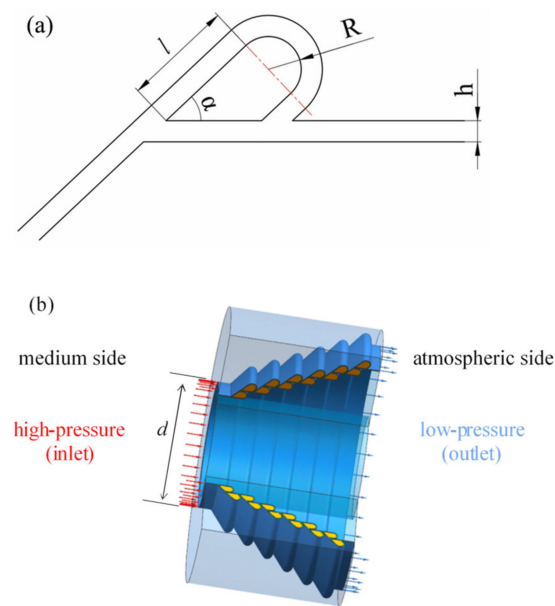
Figure 3. Physical model of the new seal. (**a**) Single-stage sealing structure diagram. (**b**) Leakage model of stepped self-impact seal [25].

2.3.2. Efficient Design

In order to achieve the efficient arrangement of seal stages, after repeated research finally proposed a cascading structure, as shown in Figure 4, the structure can cleverly realize the convenient plug and pull the assembly of the suspending pillar along the axial direction, greatly improve the positioning and assembly accuracy of each component and coordinate the arrangement of axial and radial seal stages. The specific assembly process is also convenient: similar to rolling bearings, dynamic ring and suspension column can be assembled externally as a whole. The suspension columns in different positions (distinguished by colour) are placed on the moving ring or the static ring and then the static and moving ring can be paired together. The dynamic ring is connected to the shaft by keys, setting screws, etc., and the static ring is connected to the shell by positioning the pins or interference fit, etc. The suspended column can be connected to the dynamic ring by 4–5 setting screws, and the present study has also considered designing local micro-convex body on the suspended column to achieve a more convenient interference assembly mode (the specific scheme is forming a patent technology). If more stages are needed in the axial direction, the multi-column series arrangement can be further planned.
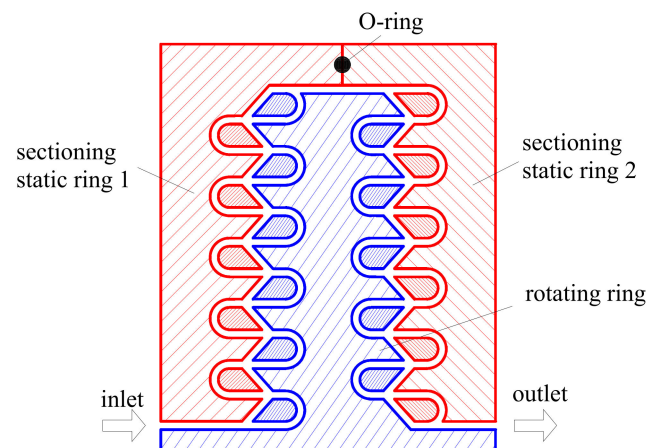
Figure 4. Self-impact seal of the cascade structure design.

2.3.3. Stage Unit Design

Figure 5 shows the size diagram of the cascade structure progression unit, defining the inlet distance *m*, outlet distance *n* and flow distance *l* and defining the interleaving value *e* to identify the axial interleaving position. When *e* = 0, the structure is symmetric and the three bifurcation channels at the staggered position are uniform; when *e* < 0, the axial direction of the structure becomes narrow and the backflow channel is located behind other bifurcation channels; and when *e* > 0, the axial direction of the structure becomes wider and the backflow channel is in front of other bifurcation channels. It can be seen that the position of the backflow channel is determined by the interleaving value. Considering the influence of the seal spacing *h*, the interleaving ratio *k* = *e*/*h* is defined as a dimensionless representation value to measure the positive and negative interleaving amount of the stage unit.
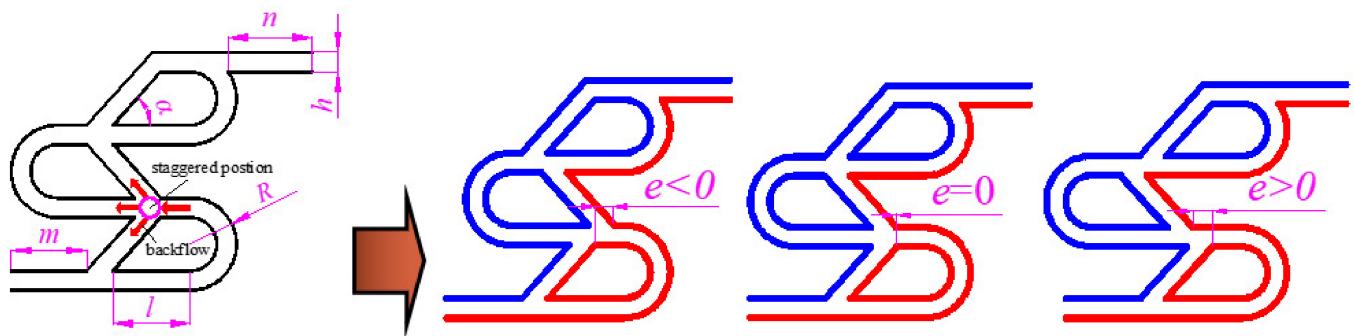

Figure 5. Dimensions of cascade structure stage unit.

3. Numerical Model

3.1. Calculation Parameters

Calculation parameters of the proposed seal are shown in Table 1. The interval range of some parameters is limited. In order to study the influence of one parameter on the sealing performance, it is necessary to analyse the other parameters under the premise that they are relatively unchanged. The relative invariants set in the right column are the specific values of other parameters when studying the change law of a specific parameter.

Table 1. Calculation parameters of proposed self-impact seal.

Parameters	Specification	Relative Fixed Value
Sealing shaft diameter *d* [mm]	76	76
Seal spacing *h* [μm]	30–300	150
Turning radius *R* [mm]	2.25	2.25
Flow distance *l* [mm]	5.50	5.50
Medium pressure P_{in} [MPa]	0.10–1	0.50
Rotation speed *N*/rpm	5000–50,000	20,000
Number of seal stage *Z*	2–20	8
Shunt angle *α*/°	40–60	48

3.2. Computational Analysis Model

3.2.1. Basic Assumptions

Water and air were selected as liquid and gas representatives in this study, respectively, and the following assumptions were introduced for the sealing model:

(1) the medium between the three-dimensional tubular channels is a continuous medium flow [26];

(2) the fluid behaviour in the Tesla valve structure belongs to the typical internal strong curvature separation flow [27], and the flow state of the self-impact sealing flow field is turbulent;

(3) the temperature and viscosity of the fluid within the flow field remain constant [28];

(4) the lubrication layer in the flow field is closely adsorbed to the pipe wall with no slip generated;

(5) the effect of seal channel deformation on fluid flow is disregarded;

(6) the effect of cavitation is disregarded;

(7) the surface of the pipe is theoretically smooth.

3.2.2. Governing Equation

The mass conservation equation, momentum conservation equation and energy conservation equation must be satisfied for fluid flow in a self-impingement seal. In order to facilitate the analysis of each governing equation, the general form of the fundamental equations is adopted. By applying the basic assumptions, the steady-state numerical simulations of the proposed seal were performed using the ANSYS CFD FLUENT software. Taking the energy conservation equation as an example, the governing equation is as follows:

$$\frac{\partial(\rho u T)}{\partial x} + \frac{\partial(\rho v T)}{\partial y} + \frac{\partial(\rho w T)}{\partial z} = \frac{\partial}{\partial x}\left(\frac{k}{c}\frac{\partial T}{\partial x}\right) + \frac{\partial}{\partial y}\left(\frac{k}{c}\frac{\partial T}{\partial y}\right) + \frac{\partial}{\partial z}\left(\frac{k}{c}\frac{\partial T}{\partial z}\right) + S_T \quad (1)$$

where

ρ—medium density of the fluid

u, v and w—axial, radial and tangential fluid flow velocities, respectively

T—fluid temperature

c—specific heat capacity

U—heat transfer coefficient

c—specific heat capacity

S_T—viscous dissipative item [29]

3.2.3. Boundary Conditions

The following two types of boundary conditions were used in the simulation.

① Mandatory boundary condition: at the inlet, $p = P_{in}$ (medium pressure); at the outlet, $p = P_o$ (atmospheric pressure).

② Wall boundary conditions: the wall function method was used in the near wall area. The solid wall was set as an adiabatic, smooth and non-slip boundary and the airflow direction was perpendicular to the inlet section.

In this study, the k–ω turbulence model in the Fluent software was selected for the solution. Using this model, the flow in the buffer zone near the wall is accounted for when calculating the abovementioned flow field type; additionally, the inverse pressure gradient and strong curvature flow field can be calculated more accurately [27,30].

The SIMPLE algorithm was used for subrelaxation iteration calculation. The diffusion term was discretised via central difference; the convection term was calculated via a second-order upwind scheme; and the iteration accuracies of continuity equation, momentum equation and energy equation were all set to 10^{-6}.

3.2.4. Mesh Division and Boundary Setting

The UG software was used to conduct the full-size modelling of the three-dimensional leakage channel of the proposed seal. Subsequently, the model was imported into Fluent Meshing for meshing. By performing an overall control and adjusting the parameters in Surface Mesh Controls, the meshing and local encryption of the model were achieved, and the meshing results are shown in Figure 6a.
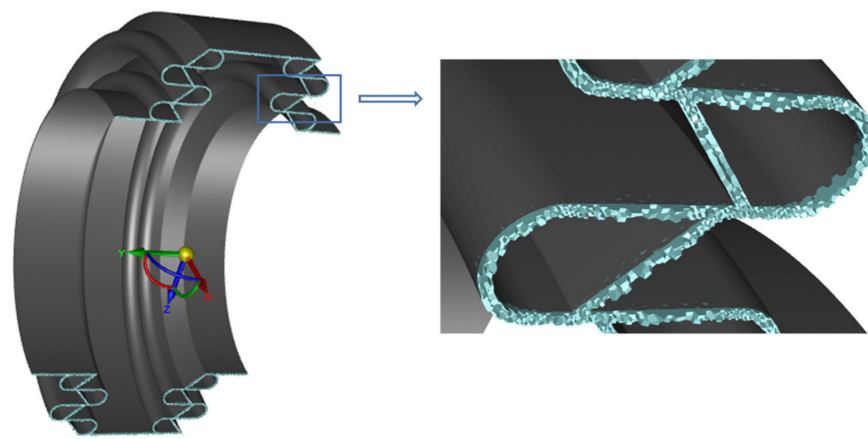
(**a**) Mesh model
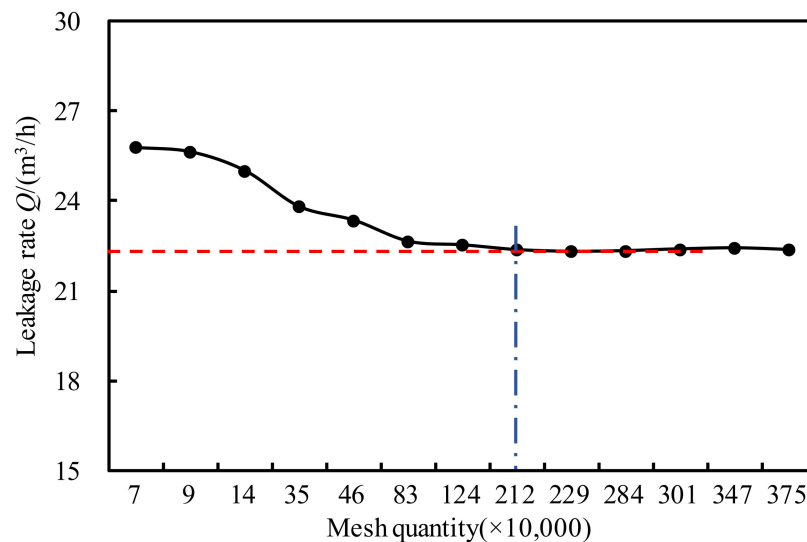


(**b**) Effects of grids number on leakage

Figure 6. Mesh generation.

Mesh-independent verification was performed using leakage as the index parameter. The calculation results, as presented in Figure 6b, show that the calculation for the proposed sealing necessitates a high grid accuracy and that the calculation results can be stabilised only when the number of grids reaches at least 2 million.

4. Calculation Results and Analysis

4.1. Flow Field Characteristics

The pressure and velocity nephogram of a gas medium (air) corresponding to different stages positions are shown in Figure 7a,b, respectively, where a local magnification is performed at the intersection area of fluid flow. As shown, significant pressure and velocity fluctuations occurred in both intersection areas and the local flow became unstable due to collisions among fluids, bifurcation flows, etc. When the gas enters the seal gap, the pressure decreases slowly after the impact of each seal stage; meanwhile, the flow velocity increased and then decreased, indicating that the velocity increase caused by the pressure difference was gradually offset and suppressed by the stepwise throttling effect after the gas entered. In addition, a secondary flow was generated at the convergence corner, which resulted in energy loss and hence reduced pressure and velocity, thereby facilitating the sealing function.

(**a**) Static pressure nephogram

(**b**) Velocity nephogram
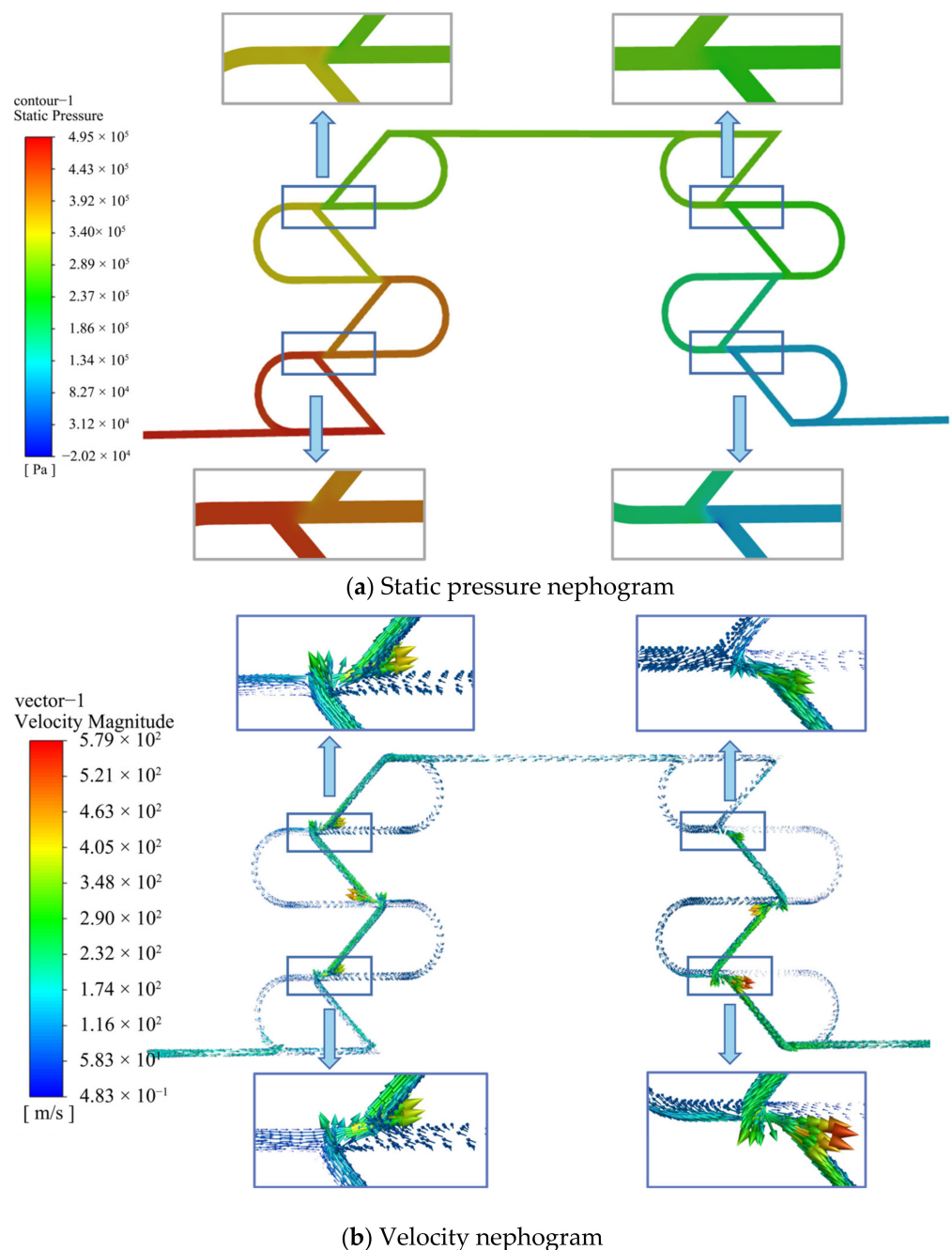
Figure 7. Flow field characteristics. (h = 0.3 mm, P_{in} = 0.2 MPa, N = 20,000 rpm, Z = 8).

4.2. Calculation of Optimal Design Parameters

Research [30] shows that the impact blocking effect of a two-dimensional flat Tesla valve is more effective for low viscous fluid. In view of this, air medium is selected for preliminary optimization analysis of design parameters.

(1)   Optimal interleaving ratio

Figure 8 shows the influence law of interleaving ratio changes on seal leakage under different seal spacing. It can be seen that the leakage is the largest in negative interleaving, which is always at a high level, possibly because negative interleaving leads to backflow channel lag. When there is no interleaving (k = 0), the leakage is between negative interleaving and positive interleaving and then decreases first and then increases with the increase in the positive interleaving ratio. The variation trend of different seal spacing is similar and the leakage is the smallest when the interleaving ratio k = 2.
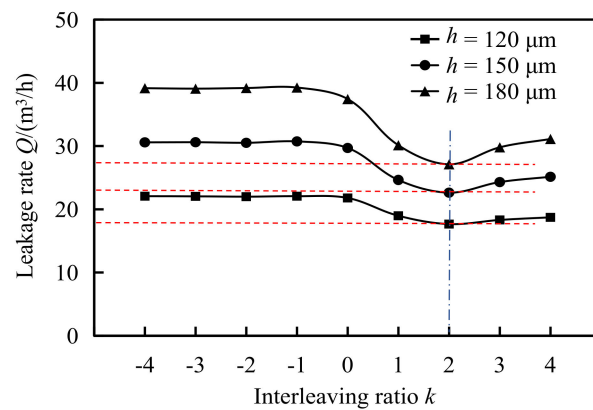
Figure 8. Effect of interleaving ratio on seal leakage. (h = 150 μm, P_{in} = 0.5 MPa, N = 20,000 rpm, Z = 8).

(2)   Optimal shunt angle

The shunt angle can determine the position of the suspending pillar and the sealing channel. The study shows that the optimal shunt angle of a two-dimensional flat Tesla valve is between 45° and 48°. As can be seen from Figure 9, the influence of shunt angle on the leakage is not obvious. With the increase in the shunt angle, the leakage tends to increase slowly. Considering that when the shunt angle decreases, the suspending pillar thickness becomes thinner and the strength decreases, which is not conductive to strength support under intense working conditions. In view of this, the selection of the new seal shunt angle is consistent with that of the two-dimensional flat Tesla valve and the appropriate choice is between 45°and 48°.
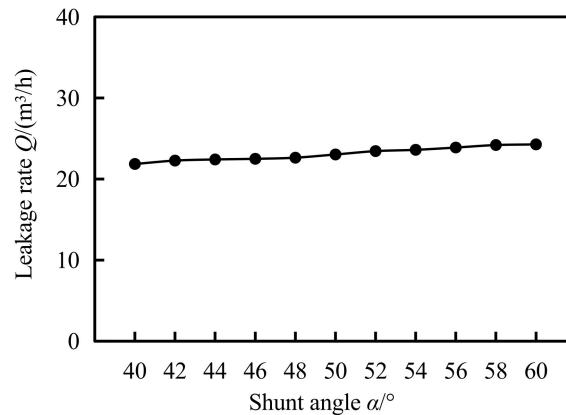
Figure 9. Effect of shunt angle on seal leakage (h = 150 μm, P_{in} = 0.5 MPa, N = 20,000 rpm, Z = 8, k = 2).

(3)   Optimal radius of suspending pillar

The radius of the suspending pillar determines the actual size of the backflow radius and the seal stage. For a given size, the larger the radius of the suspending pillar, the less the seal stage will be and vice versa. The abscissa shown in Figure 10 is the maximum seal stage corresponding to a different suspending pillar radius when the radial size is limited to 50 mm. It can be seen that with the reduction of the suspending pillar radius the maximum seal stages accommodated increases and the leakage slowly decreases. It can be seen that reducing the suspending pillar radius and increasing the number of sealing stages within a limited size can improve the leakage inhibition ability. However, with the decrease in the suspending pillar radius and the increase in the sealing stages, the strength of the suspending pillar will be further reduced and the processing difficulty of the suspending pillar and the seal rings will be increased. Therefore, the suspending pillar should not be too small. In this paper, the recommended value range is R 2.05–2.45 mm.
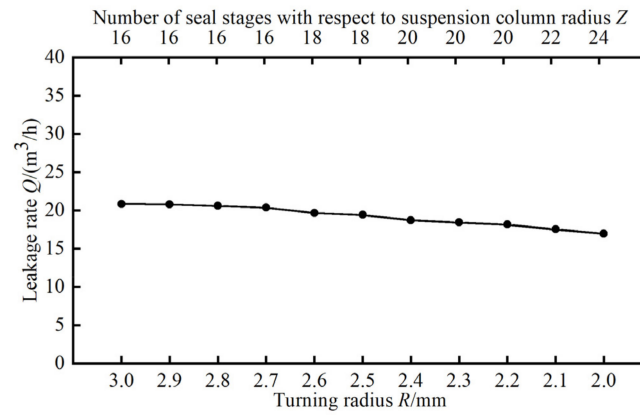
Figure 10. Effect of suspending pillar radius on seal leakage. (h = 150 μm, P_{in} = 0.5 MPa, N = 20,000 rpm, k = 2).

(4)   Optimal structure scheme

The cascade structure of the sealing includes four schemes, as shown in Figure 11a–d. Taking the 10-level seal as an example, the structure types of the static ring and the rotating ring are defined as A(a) and B(b) forms, respectively, where A and B represent the presence of winglike structure at the bottom, and a and b represent the absence of winglike structure at the bottom. Accordingly, the structural schemes of Figure 11a–d are AbbA, AbbA, AbbA and AbbA, respectively. This definition and classification is suitable for various seal stages. As shown in Figure 11e–h, they are the seal structures of stage 4, 6, 8 and 10, corresponding to the AbbA scheme.
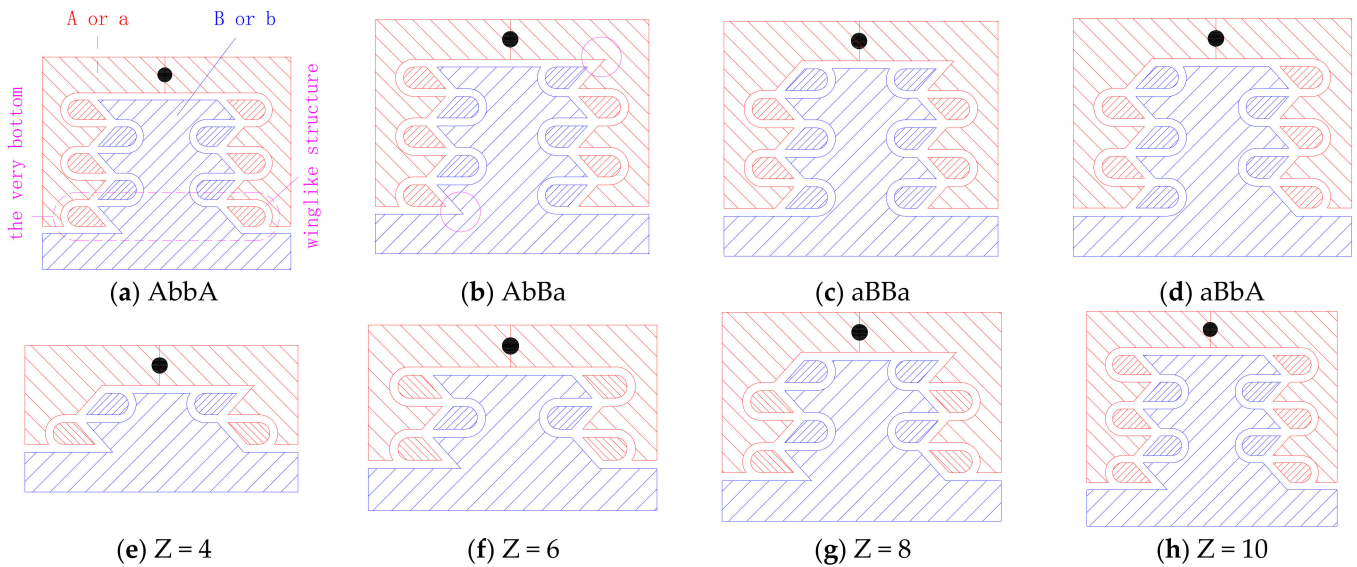
Figure 11. Cascade structure design scheme.

The calculation results of leakage under different seal stages (Z = 4, 6, 8, 10) of the four schemes were shown in Table 2. Specifically, when the stages are level 4 and level 8, the schemes are ranked as AbBa < AbBa < AbBa < AbBa < AbBa < AbBa according to the leakage size. When the stages are level 6 and level 10, the schemes are ranked as AbBa < AbBa < AbBa < AbBa < AbBa < AbBa according to the leakage size. It can be seen that the leakage performance of all schemes is consistent when the stages interval is 4 levels. The leakage of AbBa scheme is the smallest. The reason for this may be that the cascade structure on both sides of this scheme causes the incoming flow to directly block and then be shunted (see Figure 11b). In this form, the energy dissipation efficiency

is higher. Therefore, scheme AbBa can be considered as the optimal structure scheme for leakage suppression, and this structure is used in the following sections.

Table 2. Leakage of four schemes under different seal stage numbers $Q(\text{m}^3/\text{h})$.

	AbbA	AbBa	aBBa	aBbA
$Z = 4$	24.63	23.69	24.88	26.23
$Z = 6$	22.63	22.02	22.24	22.70
$Z = 8$	21.24	20.65	20.98	21.56
$Z = 10$	20.28	20.09	20.26	20.43

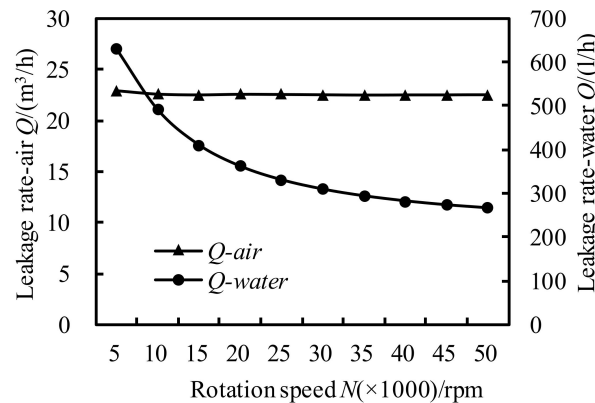*4.3. Leakage Characteristics*

(1)   Effect of operating parameters

Figure 12a,b shows the effects of pressure and speed on the leakage characteristics of the proposed seal under different media, respectively. As shown in Figure 12a, as the pressure increased, the leakage in both media indicated an increasing trend and the proposed seal almost achieved zero leakage for the air medium at zero pressure difference. Pressure affects leakage significantly, and satisfying leakage requirements under high-pressure conditions is one of the challenges of the proposed seal. As shown in Figure 12b, the rotation speed has little effect on the leakage amount when the medium is air, while when the medium is water, the leakage amount gradually decreases with the increase in the rotation speed. This may be caused by the high viscosity of the liquid, because the higher the speed, the more prominent the effect of viscous force, and the change of rotation speed has no effect on low viscosity air.
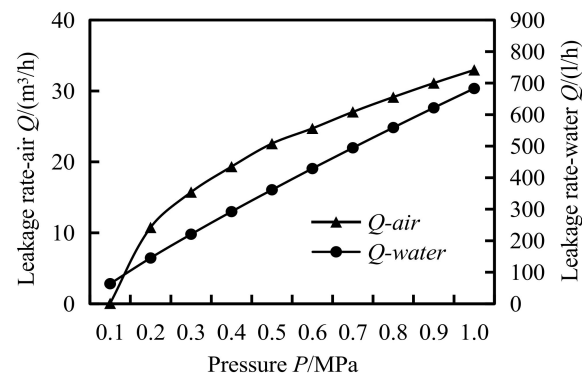

(**a**) Effects of pressure on leakage


(**b**) Effects of rotation speed on leakage

Figure 12. Effects of operating parameters on leakage rate.

(2)　　Effects of geometric parameters

Figure 13a,b shows the effect rules of seal spacing and the number of seal stages on the leakage characteristics of the proposed seal under different media, respectively. As shown in Figure 13a, the seal spacing exerted the same effect on the leakage under different media. The leakage increased significantly with the increase in seal spacing. Hence, it is clear that adjusting the seal spacing is able to effectively reduce leakage. As shown in Figure 13b, leakage rate under different media shows a decreasing trend as the number of seal stages increases. The decreasing rate of air leakage with the increase in sealing stage is higher than that of water. The leakage of water medium shows a certain fluctuation trend with the increase in seal stages (design scheme change), indicating that the throttling effect of water medium is more sensitive to the design scheme. In conclusion, the higher the number of stages, the greater the energy loss under the intersection impact and the better the effects of throttling and speed reduction, and the adjustment number of stages is also an effective way to control leakage rate.
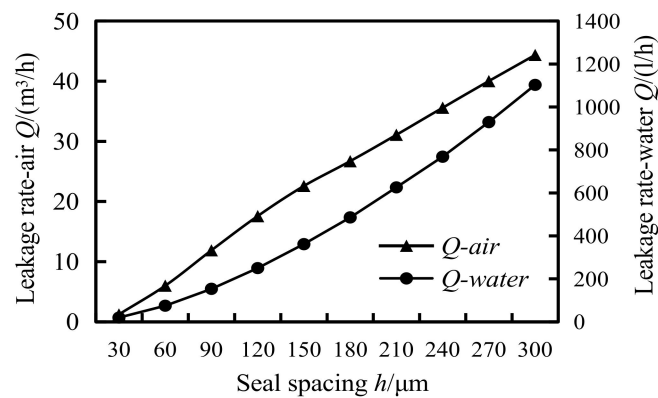
(**a**) Effects of seal spacing on leakage.
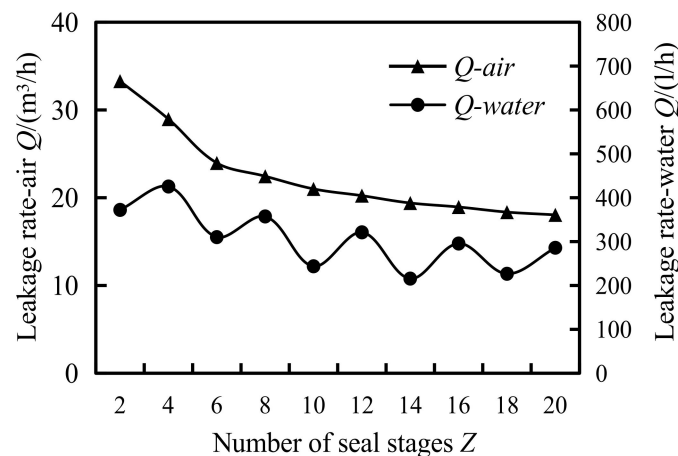
(**b**) Effects of number of seal stages on leakage.

Figure 13. Effects of geometrical parameters on leakage.

4.4. Temperaturecharacteristic

Figure 14 shows the temperature change diagram of the self-impact seal. It can be seen from the figure that the temperature of the air flow through the whole flow passage presents a step by step rising trend and the temperature change rule conforms to the action mechanism of converting kinetic energy into internal energy. It can also be seen from the temperature cloud map that the temperature change in the intersection area is significant, while the temperature change in the channel is small, which further shows the

intensity of the fluid impact in the intersection area. The local magnification of temperature distribution shows that the closer to the inner annular passage wall, the higher the air flow temperature. This is because the inner ring is a rotating element and a certain frictional effect will be generated during rotation, resulting in the temperature created near the inner ring being higher than in the other parts. To sum up, the energy exchange in the sealing micro-scale flow field is warm and local high temperature should be considered when selecting materials. It has been suggested that titanium alloy should be chosen as the new type of sealing dynamic and static ring material in high speed and high pressure situations, which has certain advantages in terms of high temperature, comprehensive mechanical properties and cost.
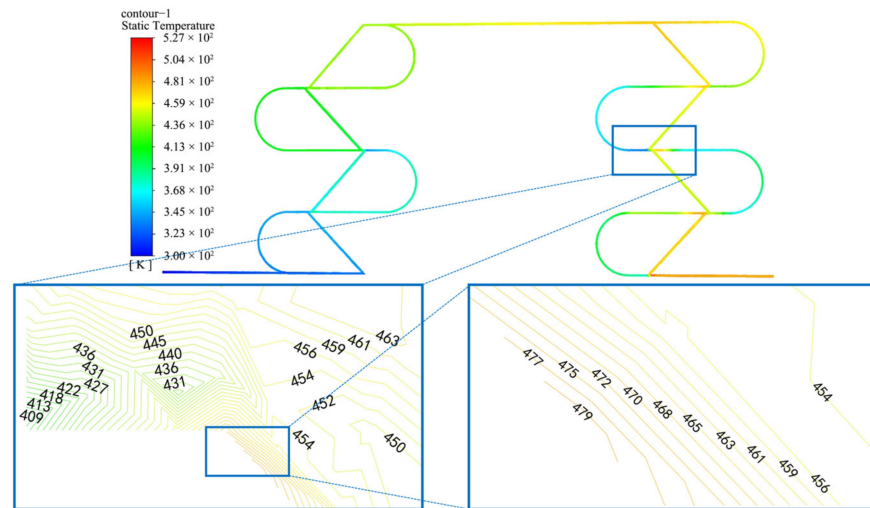

Figure 14. Temperature cloud map (h = 500 μm; P = 0.5 MPa; N = 20,000 rpm; Z = 8).

4.5. Leakage Characteristic

To achieve the practical application of the proposed seal, the latter should be fabricated to satisfy the leakage standard requirements under certain pressure difference and rotation speed conditions. In this regard, the dynamic leakage index (for the compressors) specified in the technical conditions of a dry gas seal was used as the standard to design and calculate the proposed seal [31], as shown in Table 3.

Table 3. Standard value for dynamic leakage of dry gas seals for compressors Q_{min} (m³/h).

Sealing Gas Pressure P/MPa	Rotation Speed N/rpm	Seal Diameter D/mm $60 \leqq d \leqq 90$
0.5 < P ≦ 1.0	>1000~3000	≦0.45
	>3000~7000	≦0.5
	>7000~13,000	≦0.7
	>13,000~18,000	≦0.8

The dimensions and operating parameters are listed in Table 1. Based on Table 3, N = 18,000 rpm, d = 76 mm, P = 0.6 MPa and the standard leakage Q_{min} = 0.8 m³/h. As shown in the previous section, leakage can be effectively controlled by adjusting the seal spacing and number of seal stages. Figure 15 shows the calculated leakage for the self-impact sealing structure under the different numbers of seal stages and spacings with 0.6 atm pressure difference. It was observed that as the number of seal stages increased, the corresponding seal spacing for achieving standard leakage became larger. Based on data fitting, when the number of seal stages were Z = 8, 12 and 16, the corresponding critical sealing space required to satisfy the leakage standard was h = 22, 24 and 26 μm, respectively, which were significantly higher than those of the dry gas seal film condition

(2–5 μm); this feature is able to significantly reduce the probability of sealing pair contact, thereby improving sealing stability.
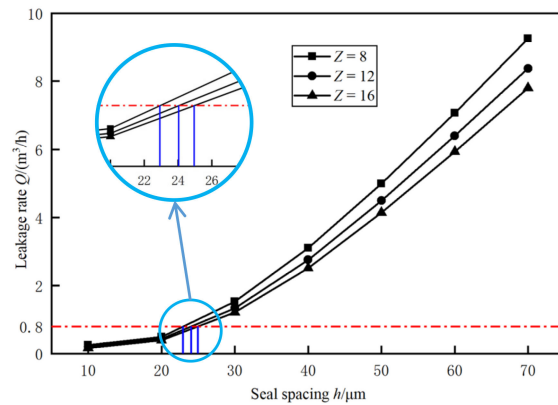

Figure 15. Seal spacing for self-impact seal under standard leakage conditions.

4.6. Comparative Analysis of Various Types of Non-Contact Seals under the Same Working Conditions

To compare and analyse the performance of the new seal and various typical non-contact seals under the same working conditions, various seal analysis models are established based on the same width, axle diameter, spacing, pressure, speed and medium, including the clearance seal, labyrinth seal, screw seal and new self-impact seal. The structure and calculation parameters of each model are shown in Table 4.

Table 4. Model structure and calculation parameters of each non-contact seal.

(a) clearance seal [32]	**(b) labyrinth seal [33]**
(c) screw seal [34]	**(d) self-impact seal**

Calculation Parameters	
Sealing medium	Air
Seal axial width L/mm	35
Sealing shaft diameter d/mm	76
Seal spacing h/μm	150

Table 4. *Cont.*

Calculation Parameters	
Outer diameter of screw seal D/mm	76.78
Tooth top width of screw seal b_e/mm	3.48
Groove width of screw seal b_g/mm	3.48
Helix angle β/°	5
Number of spiral heads i	3
Seal pitch of labyrinth seal s_1/mm	2
Tooth thickness of labyrinth seal s_2/mm	0.3
Clearance of labyrinth seal c_1/mm	0.1
Tooth height of labyrinth seal h_l /mm	2.45
Inclination angle of labyrinth seal θ/°	12
Tooth number of labyrinth seal Z_t	17
Medium pressure P_{in}/MPa	0.5
Rotation speed N/rpm	20,000
Number of stages for self-impact seal Z	16
Shunt angle α/°	48
Turning radius R/mm	2.25
Flow distance l/mm	5.50

The calculated results are shown in Table 5. It can be seen that under the same working conditions, compared with the labyrinth seal, screw seal and clearance seal, the self-impact seal is able to reduce leakage by 35.14%, 53.59% and 58.49%, respectively. Moreover, the dynamic and static rings of the self-impact seal are fixed rigidly, and the seal spacing formed is a fixed gap, which has a better ability to resist vibration or impact. In general, the overall sealing performance of the self-impact seal is significantly better than that of other non-contact sealing forms. In actual working conditions, it is similar to a labyrinth and dry gas seal, which has certain requirements regarding the cleanliness of the gas medium and large particles in the medium should be avoided. The presence of larger particles may scratch the dynamic ring or suspension column and too many particles will hinder the flow path, causing the seal to fail. Moreover, the higher temperature and too many stages can also easily cause the medium to coke, scale and crystallize and thus destroy the sealing function. The self-impact seal model proposed in this paper has only been simulated at present and will be verified by specific experiments in the future. More exploration and research is needed in the future for the practical application of the new seal.

Table 5. Comparison of calculation results of leakage of several non-contact seals.

Seal Type	Air Leakage Rate (m^3/h)	Relative Reduction Ratio
Labyrinth seal	29.60	35.14%
Screw seal	41.37	53.59%
Clearance seal	46.25	58.49%
Self-impact seal	19.20	-

Relative reduction ratio = (leakage of other seal types-leakage of self-impact seal)/leakage of other seal types.

5. Conclusions

1. The inner and outer rings of the proposed seal design can be rigidly fixed by relying on other components. Furthermore, the rings maintained a stable clearance to enable non-contact operation under the sealing function. Consequently, the ability of the sealing pair in resisting axial/radial vibrations improved significantly. Furthermore,

the sealing condition was not limited by the rotation speed and no stopping of the auxiliary sealing device was required.

2. Theoretically, the standard leakage or even zero leakage of the proposed seal can be achieved if the number of seal stages is sufficiently high. The proposed seal exhibited an improved leak suppression effect in low-pressure and high-viscosity media, with multiple seal stages and small seal spacings; furthermore, it was less affected by the rotation speed and media density. The reverse throttling effect was the most sensitive to pressure and seal spacing changes and it remained insensitive to the rotation speed and density.

3. Under the same operating conditions, when the proposed seal achieved the same standard of leakage, the corresponding seal spacing was several or dozens of times that of the dry gas seal, which was conducive to reducing the direct contact risk of the sealing pair and significantly improved the operation stability of the non-contact seal.

4. The proposed symmetrical seal structure is able to achieve the same cross-sectional area at the inlet and outlet interfaces; as such, leakage will not increase when the number of seal stages is increased, which improves the throttling effect. The segmented design of the outer ring is able to solve the assembly problem. This design idea can provide a theoretical reference for the further optimisation and engineering development of the proposed impact seal.

Nomenclature

R	Turning radius [mm]
l	Flow distance [mm]
α	Shunt angle [°]
d	Sealing shaft diameter [mm]
h	Seal spacing [μm]
m	Inlet distance [mm]
n	Outlet distance [mm]
e	Interleaving value [mm]
$k(e/h)$	Interleaving ratio
P_{in}	Medium pressure [MPa]
Z	Number of seal stages
N	Rotation speed [rpm]
ρ	Medium density of the fluid [kg/m^3]
u	Axial fluid flow velocities [m/s]
v	Radial fluid flow velocities [m/s]
w	Tangential fluid flow velocities [m/s]
T	Fluid temperature [K]
U	Heat transfer coefficient
c	Specific heat capacity [J/kg·K]
S_T	Viscous dissipative item

Q	Leakage rate [m³·h⁻¹]
Q_{min}	Standard value for dynamic leakage of dry gas seals for compressors [m³·h⁻¹]
P	Sealing gas pressure [MPa]
L	Seal axial width [mm]
D	Outer diameter of screw seal [mm]
b_e	Tooth top width of screw seal [mm]
b_g	Groove width of screw seal [mm]
β	Helix angle [°]
i	Number of spiral heads
s_1	Seal pitch of labyrinth seal [mm]
s_2	Tooth thickness of labyrinth seal [mm]
c_1	Clearance of labyrinth seal [mm]
h_l	Tooth height of labyrinth seal [mm]
θ	Inclination angle of labyrinth seal [°]
Z_t	Tooth number of labyrinth seal

References

1. Dindorf, R.; Wos, P. A numerical solution of temperature distribution in the clearance and the sealing rings of the non-contact face seal. *J. Phys. Conf. Ser.* **2021**, *1741*, 012032. [CrossRef]
2. Zaniewski, D.; Klimaszewski, P.; Klonowicz, P.; Lampart, P.; Witanowski, Ł.; Jędrzejewski, Ł.; Suchocki, T.; Antczak, Ł. Performance of the honeycomb type sealings in organic vapour microturbines. *Energy* **2021**, *226*, 120242. [CrossRef]
3. Androsovich, I.V.; Siluyanova, M.V. Optimization of labyrinth seals in gas-turbine engines. *Russ. Eng. Res.* **2021**, *41*, 360–362. [CrossRef]
4. Wang, Y.; Sun, J.J.; Hu, Q.; Wang, D.; Zheng, X. Orientation effect of orderly roughness microstructure on spiral groove dry gas seal. *Tribol. Int.* **2018**, *126*, 97–105. [CrossRef]
5. Bai, S.X.; Hao, J.L.; Yang, J.; Song, Y. Gas-liquid mass transfer behavior of upstream pumping mechanical face seals. *Materials* **2022**, *15*, 1482. [CrossRef]
6. Zhang, W.W.; Chen, H.Z.; Jiang, W.K.; Liu, R.; Jiang, S. A Spiral Seal Method in the Lunar Regolith for Chang'E-5 Drill: Seal Design and Experiment. *IEEE Access* **2019**, *7*, 11378–11386. [CrossRef]
7. Zhou, X.J.; Chen, C.L.; Li, J.H.; Wu, Y. Study on radial clearance sealing performance of graphite ring. *J. Press. Vessel Technol.* **2021**, *143*, 031703–031711. [CrossRef]
8. Zhi, D.; Li, S.X.; Zhang, Q.X.; Cai, J.N. Experimental research on new type of the centrifugal seal for sealing gas. *Fluid Mach.* **2012**, *40*, 12–15. [CrossRef]
9. Mitamura, Y.; Nishimura, I.; Yano, T. Thermal analysis of a miniature magnetic fluid seal installed in an implantable rotary pump. *J. Magn. Magn. Mater.* **2022**, *548*, 168977. [CrossRef]
10. Nikola, T. Valvular Conduit. US1329559, 3 February 1920.
11. Forster, F.K.; Bardell, R.L.; Afromowitz, M.A.; Sharma, N.R.; Blanchard, A. Design, fabrication and testing of fixed-valve micropumps. In Proceedings of the 1995 ASME International Mechanical Engineering Congress and Exposition, San Francisco, CA, USA, 12–17 November 1995.
12. Mohammadzadeh, K.; Kolahdouz, M.E.; Shirani, E.; Shafii, M.B. Numerical investigation on the effect of the size and number of stages on the Tesla microvalve efficiency. *J. Mech.* **2013**, *29*, 527–534. [CrossRef]
13. Truong, T.Q.; Nguyen, N.T. Simulation and optimization of Tesla valves. *Nanotechnology* **2003**, *1*, 178–181.
14. Gamboa, A.R.; Morris, C.J.; Forster, F.K. Improvements in fixed-valve micropump performance through shape optimization of valves. *J. Fluids Eng.* **2005**, *127*, 339–346. [CrossRef]
15. Thompson, S.M.; Ma, H.B.; Wilson, C. Investigation of a flat-plate oscillating heat pipe with Tesla-type check valves. *Exp. Therm. Fluid* **2011**, *35*, 1265–1273. [CrossRef]
16. Thompson, S.M.; Paudel, B.J.; Jamal, T.; Walters, D.K. Numerical investigation of multistaged Tesla valves. *J. Fluids Eng.* **2014**, *136*, 081102. [CrossRef]
17. Wang, C.T.; Chen, Y.M.; Hong, P.A.; Wang, Y.T. Tesla valves in micromixers. International Jouresign and operation of a Tesla-type valve for pulsating heat pipes. *Sci. Int. J. Heat Mass Transf.* **2017**, *105*, 1–11. [CrossRef]
18. Vries, S.D.; Florea, D.; Homburg, F.; Frijns, A. Design and operation of a Tesla-type valve for pulsating heat pipes. *Sci. J. Heat Mass Transf.* **2017**, *105*, 1–11. [CrossRef]
19. Jin, Z.J.; Gao, Z.X.; Chen, M.R.; Qian, J.-Y. Parametric study on Tesla valve with reverse flow for hydrogen decompression. *Int. J. Hydrogen Energy* **2018**, *43*, 8888–8896. [CrossRef]
20. Qian, J.Y.; Chen, M.R.; Liu, X.L.; Jin, Z.-J. A numerical investigation of the flow of nanofluids through a micro Tesla valve. *J. Zhejiang Univ. —Sci. A Appl. Phys. Eng.* **2019**, *29*, 50–60. [CrossRef]
21. Qian, J.Y.; Chen, M.R.; Gao, Z.X.; Jin, Z.-J. Mach number and energy loss analysis inside multi-stage Tesla valves for hydrogen decompression. *Energy* **2019**, *179*, 647–654. [CrossRef]

22. Wahidi, T.; Chandavar, R.A.; Yadav, A.K. Stability enhancement of supercritical CO_2 based natural circulation loop using a modified Tesla valve. *J. Supercrit. Fluids* **2020**, *166*, 105020. [CrossRef]

23. Monika, K.; Chakraborty, C.; Roy, S.; Sujith, R.; Datta, S.P. A numerical analysis on multi-stage Tesla valve based cold plate for cooling of pouch type Li-ion batteries. *Int. J. Heat Mass Transf.* **2021**, *177*, 121560. [CrossRef]

24. Shi, H.H.; Cao, Y.; Zeng, Y.N.; Zhou, Y.; Wen, W.; Zhang, C.; Zhao, Y.; Chen, Z. Wearable tesla valve-based sweat collection device for sweat colorimetric analysis. *Talanta* **2022**, *240*, 123208. [CrossRef] [PubMed]

25. Wang, Y.; Xie, X.F.; He, Y.M.; Huang, Z.X.; Xu, H.; Chai, D.Z.; Yang, H.S. Research on a new non-contact fluid seal technology based on Tesla Valve. *Tribology* **2022**. [CrossRef]

26. Yang, Z.; Xi, D.L.; Li, N.; Zhou, J. Numerical simulation and experimental channel performance evaluation of the microchannel structure. *Chem. Prog.* **2021**, *40*, 39–47. [CrossRef]

27. Xu, J.L.; Ma, H.Y.; Huang, Y.N. Nonlinear turbulence model reflecting strong flow curvature effect. *Appl. Math. Mech.* **2008**, *29*, 27–37. [CrossRef]

28. Weng, X.Y.; Yan, S.H.; Zhang, Y.; Liu, J.W.; Shen, J.F. Design, simulation and experimental study of a micromixer based on Tesla Valve structure. *Chem. Prog.* **2021**, *40*, 4173–4178. [CrossRef]

29. Versteeg, H.K.; Malalasekera, W. *An Introduction to Computational Fluid Dynamics: The Finite Volume Method*; Wiley: New York, NY, USA, 1995.

30. Zhou, R.Z.; Qiao, Y.J.; Zhang, Y.X.; Dai, Z.B. Simulation study on the performance of Tesla valve. *Phys. Exp.* **2020**, *40*, 44–50. [CrossRef]

31. *JB/T 11289-2012*; Specification for Dry Gas Seal. China Machine Press: Beijing, China, 2012.

32. Sun, K.Y.; Hao, Z.J. *Mechanical Seal Structure Legend and Application*; Chemical Industrial Press: Beijing, China, 2019.

33. Huo, C.; Sun, J.; Song, P.; Sun, W. Influence of tooth geometrical shape on the leakage and rotordynamic characteristics of labyrinth seals in a cryogenic liquid turbine expander. *Int. J. Refrig.* **2022**, *145*, 105–117. [CrossRef]

34. Ren, Z.H.; Wei, J.T.; Li, Y.C.; Xv, Y. Sealing capability and parameter optimization of screw seal. *J. Northeast. Univ. (Nat. Sci.)* **2016**, *37*, 1755–1758. [CrossRef]